

Particle Production at the SPS and the QCD Phase Diagram

Christoph Blume

Institut für Kernphysik, J.W. Goethe-Universität,
Max-von-Laue-Str. 1, D-60438 Frankfurt am Main, GERMANY

E-mail: blume@ikf.uni-frankfurt.de

Abstract. Recent results of particle production in the energy regime of the CERN-SPS are reviewed. In order to collect information on the properties of the QCD phase diagram systematic studies of the system size and the energy dependence of particle production in heavy ion collisions have been performed. Net-baryon distributions and results on strangeness production are discussed. The system size dependence of many observables can be understood in the core-corona approach, which has implications on the possibility to use system size as a control parameter to study different areas of the phase diagram. Recent attempts to search for a critical point, such as multiplicity fluctuations and the transverse mass dependence of anti-baryon/baryon ratios are reviewed.

1. Introduction

The QCD phase diagram, as it is illustrated in Fig. 1, contains a variety of theoretically predicted features. The most important one is the phase boundary separating a hadron gas and a quark gluon plasma (red dashed line in Fig. 1). Its position at vanishing baryonic chemical potential ($\mu_B = 0$) is defined by the critical temperature T_C . Even though recent attempts to calculate the exact value of T_C with lattice QCD still result in different numerical values [1, 2, 3], there is a general consensus that for $\mu_B = 0$ this transition is of the type of crossover. However, this crossover line might turn for a certain μ_B into a first order phase transition, which would result in a critical point at that position [4]. However, predictions on the location of the critical point are still very uncertain [5]. It might very well be that it does not exist at all [6]. Recently, it has been conjectured that the phase diagram might contain yet another phase, the so-called quarkyonic phase [7], which would be separated from normal hadronic matter by a different phase boundary line (blue dashed line in Fig. 1).

Experimentally, there are several control parameters available that might allow to study different regions of the phase diagram with heavy ion collisions. One is the variation of the center-of-mass energy which will force the reaction systems to follow different trajectories in the T - μ_B plane, reflected by a change of the chemical freeze-out parameters. The second control parameter is the variation of the system size, which can either be achieved by performing central collisions of nuclei of different size, or by studying centrality selected minimum bias collisions. However, whether this can be considered as a good control parameter for probing different areas of the phase diagram shall be discussed further below.

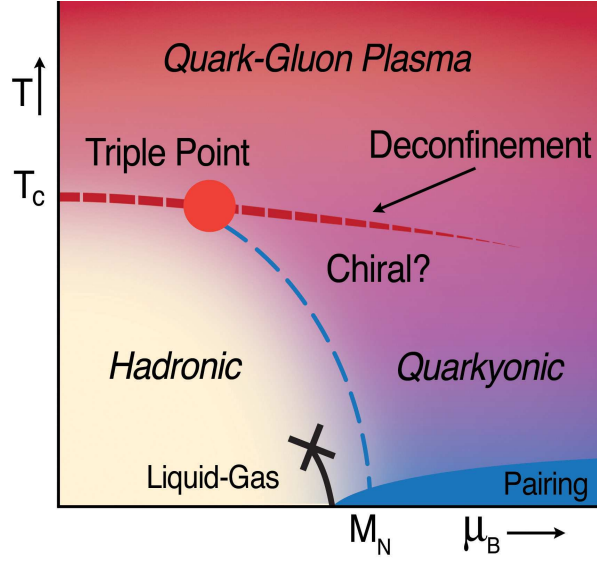


Figure 1. The phase diagram of strongly interacting matter. The picture is taken from [8].

In the following we review some results from systematic studies of particle production in heavy ion collisions performed at the CERN-SPS, and will discuss what can be learned from existing data on the experimental accessibility of different areas in the phase diagram. Finally, we also present some results from existing attempts to search for a critical point.

2. Variation of Energy

Recent results on rapidity spectra of (anti-)protons in central Pb+Pb reactions, measured at energies between 20A - 158A GeV at the SPS [9, 10], together with central Au+Au data from the AGS [11] and RHIC [12] allow to study the energy evolution of stopping. Based on the measured rapidity spectra for p , \bar{p} , Λ , $\bar{\Lambda}$, Ξ^- , and $\bar{\Xi}^+$, all corrected for feed down from weak decays, the net-baryon distributions $\bar{B} - B$ have been constructed [13]. The contribution of unmeasured baryons (n , Σ^\pm , Ξ^0) was estimated using the results of a statistical hadron gas model [14]. In the SPS energy region a clear evolution of the shape can be observed (see left panel of Fig. 2), changing from a single maximum at midrapidity towards a structure with two maxima and a dip at $y = 0$. Concurring with this evolution, also a strong change of the anti-baryon/baryon ratios takes place in the energy region of the SPS [10, 15] and thus of the baryonic chemical potential at freeze-out μ_B .

The right panel of Fig. 2 shows a comparison of the energy dependence of mid-rapidity Λ , $\bar{\Lambda}$, Ξ^- , and $\bar{\Xi}^+$ production to several models. While the transport models UrQMD1.3 [16] and HSD [17] provide a reasonable description of the Λ/π and $\bar{\Lambda}/\pi$ ratios, they are clearly below the data points in case of the Ξ^- and $\bar{\Xi}^+$. This might indicate that an additional partonic contribution is necessary to reach the production rates observed for multi-strange particles. Statistical models on the other hand, generally provide a better match to the data. These models are based on the assumption that the particle yields correspond to their chemical equilibrium value and can thus be described by the parameters temperature T , baryonic chemical potential μ_B , volume V , and, in some implementations, by an additional strangeness under-saturation factor γ_s . The curves shown in the right panel of Fig. 2, labeled SHM(B), are taken from [18] and are based on parametrizations of the $\sqrt{s_{NN}}$ dependence of T and μ_B , assuming $\gamma_s = 1$. The results of various

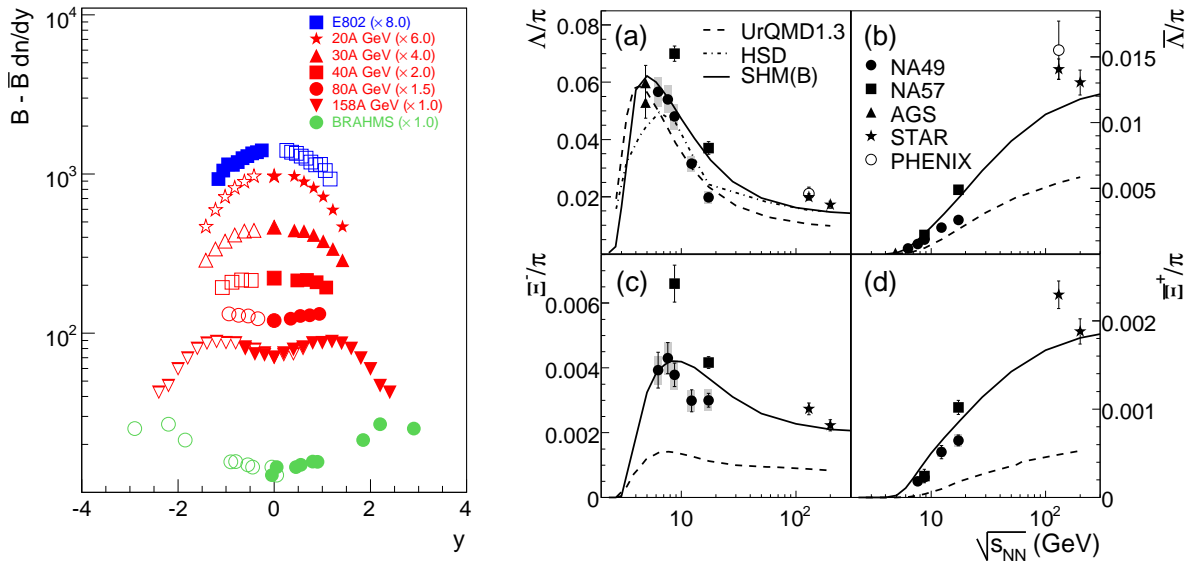


Figure 2. Left: The rapidity distributions of net-baryons at SPS energies [13, 9, 10], together with results from the AGS [11] and from RHIC [12] for central Pb+Pb(Au+Au) collisions. Right: The energy dependence of the rapidity densities dn/dy around mid-rapidity of Λ , $\bar{\Lambda}$, Ξ^- , and Ξ^+ , divided by the total pion rapidity densities ($\pi = 1.5 (\pi^- + \pi^+)$) for central Pb+Pb and Au+Au collisions [19, 20, 21, 22, 15, 23, 24, 25, 26, 27, 28, 29, 30, 31]. Also shown are results for the transport models UrQMD1.3 (dashed line) [16] and HSD (dotted line) [17], as well as a statistical hadron gas model (solid line) [18].

analysis of the measured particle abundances with statistical model approaches show that T and μ_B parameter for the SPS energy range vary over a wide region, following an universal freeze-out curve [32], and might be in the vicinity of the possible critical point location [18, 33, 34, 35]. Thus, the variation of $\sqrt{s_{NN}}$ provides a well defined way of selecting different regions in the T - μ_B plane.

3. Variation of System Size

3.1. Centrality Dependence of Net Protons

Recent data on proton and antiproton production in minimum bias Pb+Pb reactions allow to study the system size dependence of stopping. Figure 3 shows the net-proton rapidity distributions for five different centrality classes, selected from minimum bias Pb+Pb interactions at 40A (left panel) and 158A GeV (right panel) [36]. A remarkable feature of this data is that there is no drastic change with centrality of the shapes of the distributions inside the measured region at 158A GeV. However, at 40A GeV the shapes of the distributions change with centrality, going from a two-maxima structure with a narrow dip at midrapidity for central collisions to a shallow valley like distribution for peripheral collisions, similar as observed at the AGS [37].

The \bar{p}/p ratio, being directly sensitive to the baryonic chemical potential μ_B , depends much less on system size than it does depend on energy. While for the mid-rapidity ratios at 158A GeV only a change in the order of a factor of two is observed when comparing central Pb+Pb reactions ($\bar{p}/p = 0.56$, 0 – 5% most central) to very peripheral ones ($\bar{p}/p = 0.11$ for 43 – 100%), this ratio

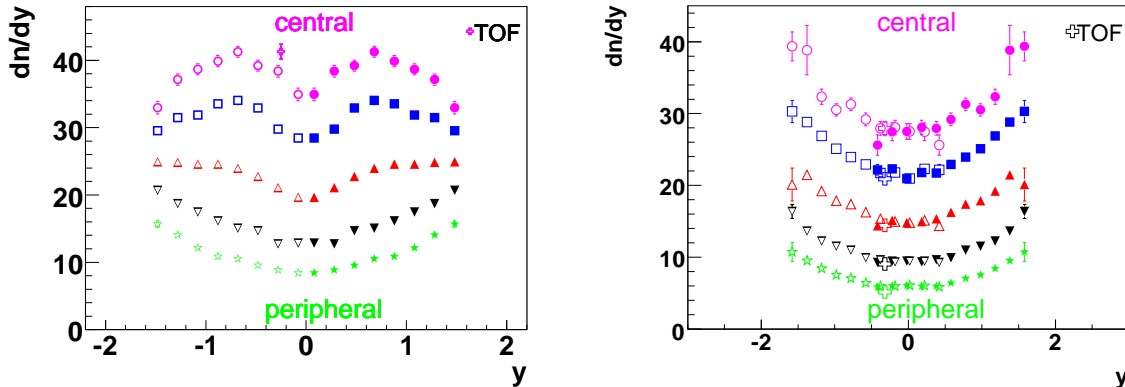


Figure 3. Net-proton rapidity distributions for Pb+Pb collisions at 40A (left) and 158A GeV (right) for different centralities as measured by the NA49 experiment [36]. The full symbols represent the measurements. The open symbols are reflected at midrapidity.

varies by a factor of 43 between central Pb+Pb collisions at 20A GeV ($\bar{p}/p = 0.0013$, 0 – 7%) and 158A GeV [10]. Thus, only a small variation of μ_B can be achieved when studying reactions of different system sizes.

3.2. Core Corona Model

It has been found that the core-corona approach is able to describe the system size dependence of particle production reasonable well [38, 39, 40, 41, 42]. In this model a nucleus-nucleus collision is decomposed into a central core, which corresponds to the large fireball produced in central A+A collisions, and a peripheral corona, that is equivalent to independent nucleon-nucleon reactions. To quantify the relative contribution of the two components, the fraction of nucleons that scatter more than once $f(N_{\text{part}})$ can be used. $f(N_{\text{part}})$ can simply be calculated with a Glauber model [43]. This quantity allows for a natural interpolation between the yields Y measured in elementary p+p ($= Y_{\text{corona}}$) and in central nucleus-nucleus collisions ($= Y_{\text{core}}$):

$$Y(N_{\text{part}}) = N_{\text{part}} [f(N_{\text{part}}) Y_{\text{core}} + (1 - f(N_{\text{part}})) Y_{\text{corona}}] \quad (1)$$

The left panel of Fig. 4 shows for example the result of this approach compared to the system size dependence of the strangeness enhancement factors E at 158A GeV [44, 45]. Here, E is defined relative to p+p reactions as baseline measurement:

$$E = \left(\frac{1}{\langle N_{\text{part}} \rangle} \frac{dN(\text{Pb+Pb})}{dy} \Big|_{y=0} \right) / \left(\frac{1}{2} \frac{dN(\text{p+p})}{dy} \Big|_{y=0} \right) \quad (2)$$

The observed rapid rise for very small systems and the subsequent saturation can naturally be described within this model.

It is interesting to observe that this approach not only works for yields, but also for dynamical quantities such as the average transverse momenta $\langle m_t \rangle - m_0$ (see right panel of Fig. 4). This suggests that the core-corona approach in general provides a reasonable way for understanding the evolution from elementary p+p to central Pb+Pb collisions.

A more differential look on the core-corona model is shown in the left panel of Fig. 5 for symmetric reaction systems. Due to their different surface to volume ratio, the N_{part} dependence

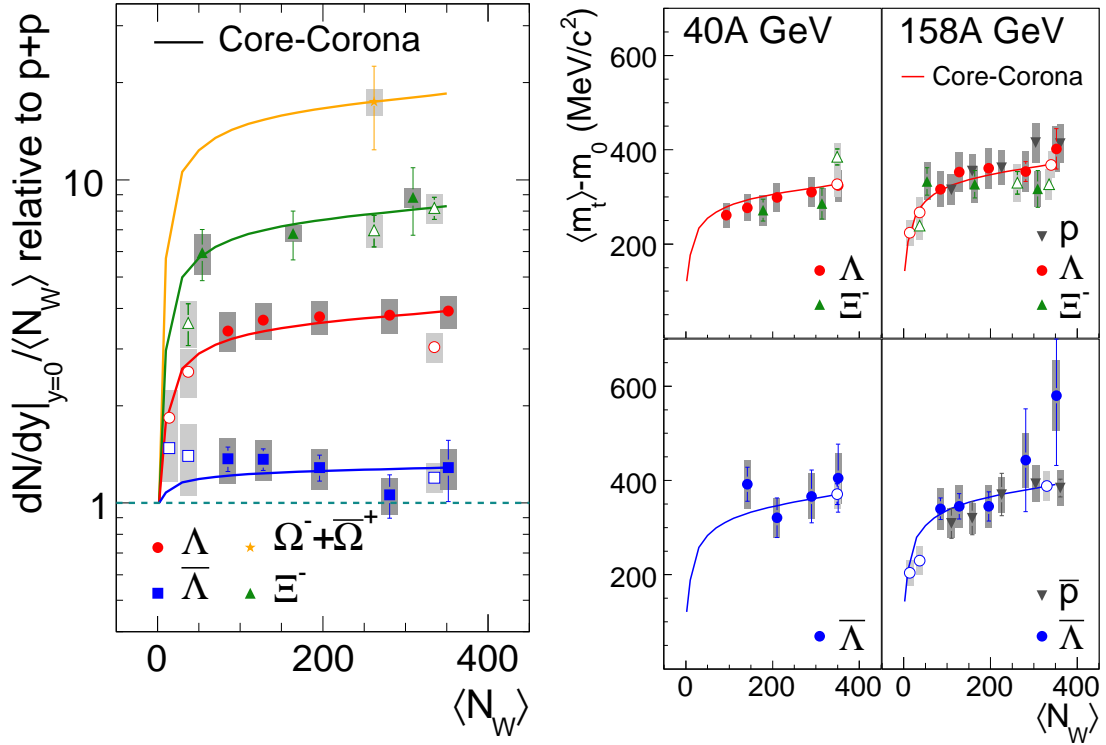


Figure 4. Left: The midrapidity yields per wounded nucleon relative to p+p yields for central C+C, Si+Si and minimum bias Pb+Pb reactions at 158A GeV [44, 45]. Right: The $\langle m_t \rangle - m_0$ values at mid-rapidity for Pb+Pb collisions at 40A and 158A GeV, as well as for near-central C+C and Si+Si reactions at 158A GeV [44]. The (anti-)proton data are taken from [46]. Also shown are the results from a fit for Λ and $\bar{\Lambda}$ with the core-corona approach (solid lines).

of $f(N_{\text{part}})$ is much steeper for smaller reaction systems than for larger ones¹. Also, the maximum value of $f(N_{\text{part}})$ depends on the size of the nuclei. E.g., while for very central Pb+Pb collisions $f_{\text{max}}(N_{\text{part}}) \approx 0.9$ can be reached, the maximum value for very central C+C reactions is $f_{\text{max}}(N_{\text{part}}) \approx 0.65$. This A dependence of f_{max} is illustrated by the dashed red line in the left panel of Fig. 5. This has the consequence that the different relative core corona contributions have to be taken into account when comparing even very central nucleus-nucleus collisions of different size. Especially, this might explain any apparent system size dependence of the chemical freeze-out parameters T and μ_B , as determined by statistical model fits to central A+A collisions of different size (e.g. [14]). Therefore, we conclude that, assuming the core-corona model is valid, the system size might not provide a good control parameter to probe different regions of the QCD phase diagram with produced fireballs of different temperature. It is more likely that one only observes a change in the relative admixture of central fireball (core) and peripheral p+p like corona, whose freeze-out parameters are different, but independent of the size of the involved nuclei.

Another interesting aspect of the core-corona model is shown in the right panel of Fig. 5. Here, the N_{part} dependence of $f(N_{\text{part}})$ is shown for asymmetric collisions. In this case quite distinct centrality dependences can be observed. While for symmetric collisions this dependence

¹ Please note that the curves shown in Fig. 4 are based on a function $f(N_{\text{part}})$ that was calculated for Pb+Pb interactions [41]. Therefore their direct comparison to the smaller systems C+C and Si+Si is not possible.

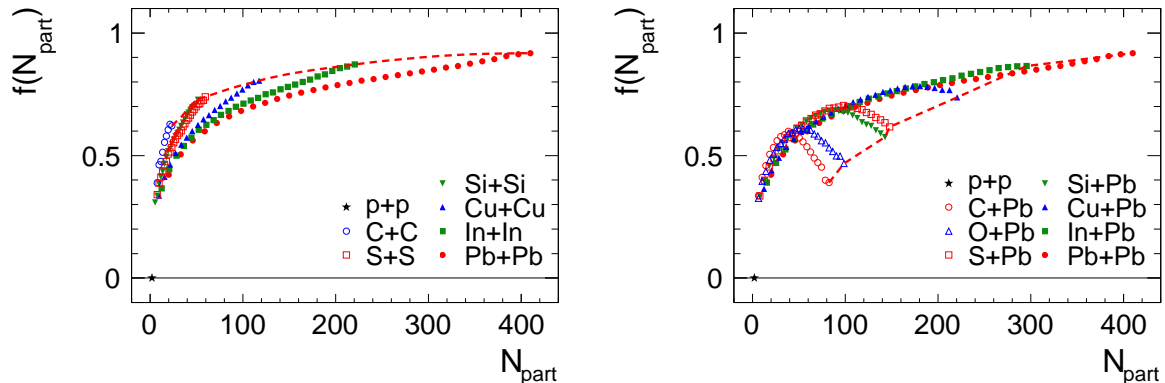


Figure 5. The fraction $f(N_{\text{part}})$ of participating nucleons that scatter more than once as a function of the number of participants N_{part} . $f(N_{\text{part}})$ was calculated with a Glauber model [43, 47]. The left panel shows results for symmetric systems, the right panel for asymmetric ones. The dashed lines connect the values for the most central collisions.

is following a continuous rise (left panel of Fig. 5), for asymmetric collision systems with a small projectile nucleus (e.g. O+Pb or Si+Pb) a rapid rise followed by a maximum and a subsequent decrease of $f(N_{\text{part}})$ is seen. Therefore, a similar centrality dependence of particle yields can be expected for these type of collisions and its measurement would constitute a test for the validity of the core-corona model.

4. Search for the Critical Point

4.1. Fluctuations

One of the observables proposed to be sensitive to the presence of a critical point in the QCD phase diagram are fluctuations of either mean transverse momentum or multiplicity [48]. If the chemical freeze-out is happening in the vicinity of the critical point, an enhancement of fluctuations might be visible. The NA49 experiment has therefore performed a systematic study of multiplicity fluctuations in very central (1% most central) Pb+Pb collisions as a function of beam energy [49]. Figure 6 shows the resulting scaled variance $\omega = \text{Var}(n)/\langle n \rangle$ as a function of baryonic chemical potential μ_B , that has been derived from statistical model fits to the particle abundances measured at the different beam energies [14].

While for all charged particles taken together ω is close to unity, it is slightly below one for negatively and positively charged particles analyzed separately, i.e. the distributions are in these cases a bit narrower than the corresponding Poissonian. However, in none of the studied charge combinations a significant energy dependence has been so far observed.

Figure 6 also shows some theoretical expectations for ω , which result from the combination of several assumptions [50]. The position of the critical point in terms of T and μ_B is taken from a lattice QCD calculation [35]. The magnitude of the fluctuations at the critical point is based on [48, 51], assuming two different correlation lengths $\xi = 3$ fm (solid line) and $\xi = 6$ fm (dashed line), while the widths of the enhancements around the critical point has been chosen according to [52] as $\sigma(\mu_B) \approx 30$ MeV. Both predictions are at variance with the data, so that up to now there is no evidence for a critical point in fluctuation measurements.

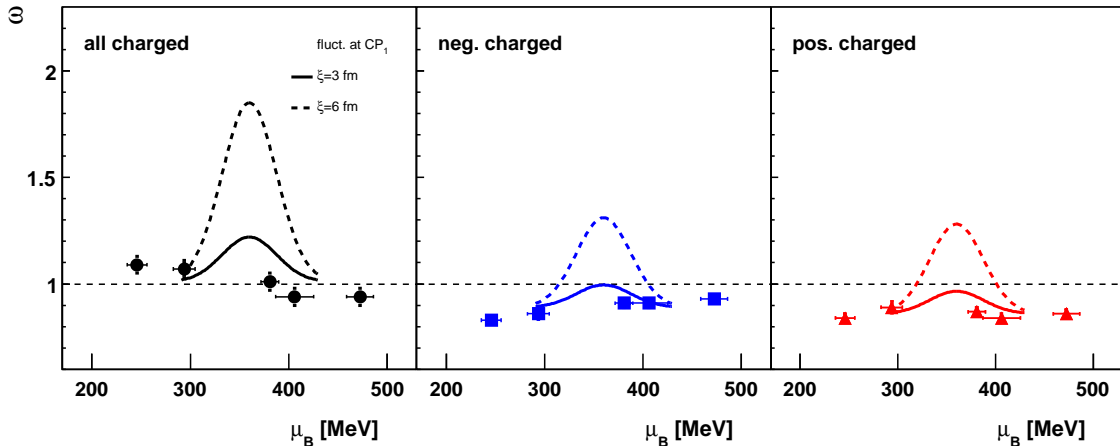


Figure 6. Energy dependence of multiplicity fluctuations, given by the scaled variance ω , for the 1% most central Pb+Pb collisions in the forward rapidity region ($1.1 < y_\pi < y_{\text{beam}}$) as measured by the NA49 experiment [49, 50]. The different beam energies are represented by the corresponding μ_B values, determined by a statistical model fit [14]. The lines correspond to predictions for for critical point (see text).

4.2. Transverse Mass Spectra of Baryons and Anti-baryons

Another possible way of detecting a critical point has been suggested in [53]. Here it was shown that the proximity of a critical point, or rather a critical area, might deform the isentropic trajectories of an expanding fireball in the T - μ_B plane, due to a focussing effect towards the critical point. As a consequence one should see a decrease of the anti-baryon/baryon ratios with increasing transverse mass, while in the absence of a critical point this ratio should rather be flat as a function of m_t .

The left panel of Fig. 7 shows the \bar{p}/p ratio versus $m_t - m_0$ for five different beam energies [10, 50]. In order to quantify any change in transverse mass dependence, a linear fit has been applied to the data. The $\bar{\Lambda}/\Lambda$ and $\bar{\Xi}^+/\Xi^-$ ratios have been analyzed in the same fashion. The resulting energy dependence of the slope parameters a is summarized in the right panel of Fig. 7. No significant energy dependence can be seen and thus this observable currently does not provide any evidence for a critical point.

5. Conclusions

In order to probe different areas in the QCD phase diagram, the variation of the center-of-mass energy can be considered as the best defined control parameter. Especially in the energy regime of the SPS a wide region in the T - μ_B plane can be explored experimentally, as is evident from the strong dependence of the chemical freeze-out parameters on the energy here. The situation is much less well defined when using the system size as control parameter. Since the system size dependences of many observables (e.g. strangeness production and $\langle m_t \rangle - m_0$) seem to be well described within the core-corona approach, it is unlikely that the freeze-out temperatures of the fireballs vary with their size. Rather one observes a change of the relative admixture of the core and corona contributions. However, the trajectories of the fireballs in the core might be always the same, irrespective of their size. Studying centrality dependences in asymmetric reaction

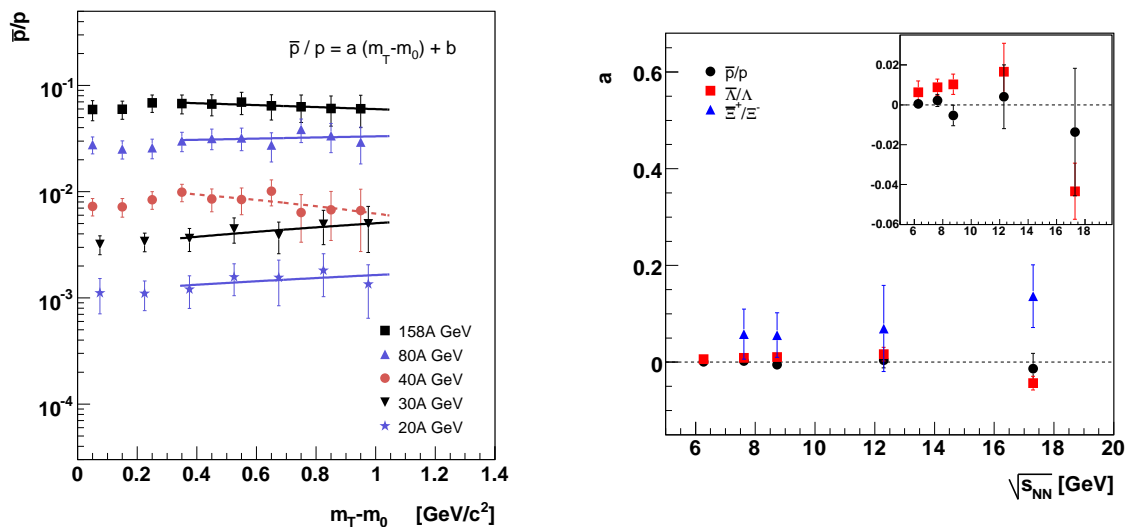


Figure 7. Left: The \bar{p}/p ratio versus the transverse mass $m_t - m_0$ [10, 50]. The solid lines show a linear fit to the ratios. Right: The energy dependence of the slope parameters a from the fits for different \bar{B}/B ratios [10, 15, 50]. The insert shows the same data with an expanded vertical scale.

systems could provide an additional experimental test of the core-corona model. In these cases this model predicts for smaller projectile nuclei a maximum in the relative core contribution for semi-central reactions, in contrast to symmetric reaction systems that reach the maximum for very central collisions.

Several attempts have been made to search within existing data for evidences of a critical point, such e.g. as fluctuations and the transverse mass dependence of anti-baryon/baryon ratios. So far non of these searches yielded a positive result. The success of future searches will on one side mainly depend on the development of more refined and differential (i.e. scale and p_t dependent) observables, that allow to distinguish effects due to a critical point from more trivial sources. On the other side, since the magnitude of these effects might be small, experimental progress on reducing systematic and statistical errors will be necessary.

Acknowledgments

The author would like to thank K. Reygers for the help with the Glauber model calculations and H. Ströbele for providing helpful comments and suggestions.

References

- [1] Aoki Y et al., 2009 *JHEP* **0906** 088.
- [2] Cheng M et al., 2006 *Phys. Rev. D* **74** 054507.
- [3] Fodor Z, *Proceedings of this WWND10 workshop*.
- [4] Stephanov M, Rajagopal K, and Shuryak E, 1998 *Phys. Rev. Lett.* **81** 4816.
- [5] Stephanov M, 2006 *PoS LAT2006* **024**.
- [6] de Forcrand P and Philipsen O, 2007 *JHEP* **0701** 077.
- [7] McLerran L and Pisarski R D, 2007 *Nucl. Phys. A* **796** 83.
- [8] Andronic A et al., 2009 *arXiv:0911.4806*.
- [9] Appelshäuser H et al. (NA49 Collaboration), 1999 *Phys. Rev. Lett.* **82** 2471.
- [10] Alt C et al. (NA49 Collaboration), 2006 *Phys. Rev. C* **73** 044910.

- [11] Ahle L et al. (E802 Collaboration), 1999 *Phys. Rev. C* **60** 064901.
- [12] Bearden I G et al., (BRAHMS Collaboration), 2004 *Phys. Rev. Lett.* **93** 102301.
- [13] Blume C (for the NA49 Collaboration), 2007 *J. Phys. G* **34** S951.
- [14] Becattini F, Manninen J, and Gaździcki M, 2006 *Phys. Rev. C* **73** 044905.
- [15] Alt C et al. (NA49 Collaboration), 2008 *Phys. Rev. C* **78** 034918.
- [16] Bleicher M et al., 1999 *J. Phys. G* **25** 1859.
- [17] Weber H, Bratkovskaya E L, Cassing W, and Stöcker H, 2003 *Phys. Rev. C* **67** 014904.
- [18] Andronic A, Braun-Munzinger P, and Stachel J, 2006 *Nucl. Phys. A* **772** 167.
- [19] Albergo S et al. (E896 Collaboration), 2002 *Phys. Rev. Lett.* **88** 062301.
- [20] Back B B et al. (E917 Collaboration), 2001 *Phys. Rev. Lett.* **87** 242301.
- [21] Ahmad S et al. (E891 Collaboration), 1996 *Phys. Lett. B* **382** 35.
- [22] Ahle L et al. (E802 Collaboration), 1998 *Phys. Rev. C* **57** R466.
- [23] Antinori F et al. (NA57 Collaboration), 2006 *J. Phys. G* **32** 427.
- [24] Antinori F et al. (NA57 Collaboration), 2004 *Phys. Lett. B* **595** 68.
- [25] Adler C et al. (STAR Collaboration), 2002 *Phys. Rev. Lett.* **89** 092301.
- [26] Adams J et al. (STAR Collaboration), 2004 *Phys. Rev. Lett.* **92** 182301.
- [27] Adcox K et al. (PHENIX Collaboration), 2002 *Phys. Rev. Lett.* **89** 092302.
- [28] Adams J et al. (STAR Collaboration), 2007 *Phys. Rev. Lett.* **98** 062301.
- [29] Adler C et al. (STAR Collaboration), 2004 *Phys. Lett. B* **595** 143.
- [30] Adams J et al. (STAR Collaboration), 2004 *Phys. Rev. Lett.* **92** 112301.
- [31] Adcox K et al. (PHENIX Collaboration), 2002 *Phys. Rev. Lett.* **88** 242301.
- [32] Cleymans J and Redlich K, 1999 *Phys. Rev. C* **60** 054908.
- [33] Becattini F, Gaździcki M, Keränen A, Manninen J, and Stock R, 2004 *Phys. Rev. C* **69** 024905.
- [34] Cleymans J, Oeschler H, Redlich K, and Wheaton S, 2006 *Eur. Phys. J. A* **29** 119.
- [35] Fodor Z and Katz S D, 2004 *JHEP* **0404** 050.
- [36] Ströbele H (for the NA49 Collaboration), 2009 *arXiv:0908.2777*.
- [37] Back B B et al. (E917 Collaboration), 2001 *Phys. Rev. Lett.* **86** 1970.
- [38] Bozek P, 2005 *Acta Phys. Polon. B* **36** 3071.
- [39] Becattini F and Manninen J, 2008 *J. Phys. G* **35** 104013.
- [40] Becattini F and Manninen J, 2009 *Phys. Lett. B* **673** 19.
- [41] Aichelin J and Werner K, 2009 *Phys. Rev. C* **79** 064907.
- [42] Werner K, *Proceedings of this WWND10 workshop*.
- [43] Glauber R J, 1955 *Phys. Rev.* **100** 242.
- [44] Anticic T et al. (NA49 Collaboration), 2009 *Phys. Rev. C* **80** 034906.
- [45] Blume C (for the NA49 Collaboration), 2008 *J. Phys. G* **35** 044004.
- [46] Anticic T et al. (NA49 Collaboration), 2004 *Phys. Rev. C* **69** 024902.
- [47] Miller M L, Reygers K, Sanders S J, and Steinberg P, 2007 *Ann. Rev. Nucl. Part. Sci.* **57** 205.
- [48] Stephanov M, Rajagopal K, and Shuryak E V, 1999 *Phys. Rev. D* **60** 114028.
- [49] Alt C et al. (NA49 Collaboration), 2008 *Phys. Rev. C* **78** 034914.
- [50] Grebieszko K (for the NA49 Collaboration), 2009 *Nucl. Phys. A* **830** 547C.
- [51] Stephanov M, *private communication*.
- [52] Hatta Y and Ikeda T, 2003 *Phys. Rev. D* **67** 014028.
- [53] Askawa A, Bass S A, Müller B, and Nonaka C, 2009 *Phys. Rev. Lett.* **101** 122302.

